

Cite this article as: Wang Yupeng, Li Siying, Ma Tengfei, et al. Enhancement in Mechanical Properties of TiAl Alloys by In-Situ Precipitation of Hybrid TiB₂-Ti₂AlN[J]. Rare Metal Materials and Engineering, 2024, 53(12): 3329-3337. DOI: 10.12442/j.issn.1002-185X.20240001.

ARTICLE

Enhancement in Mechanical Properties of TiAl Alloys by In-Situ Precipitation of Hybrid TiB₂-Ti₂AlN

Wang Yupeng¹, Li Siying¹, Ma Tengfei¹, Wang Xiaohong¹, Dong Duo^{1,2}, Zhu Dongdong^{1,2}

¹Key Laboratory of Air-Driven Equipment Technology of Zhejiang Province, Quzhou University, Quzhou 324000, China; ²School of Materials Science and Engineering, Taizhou University, Taizhou 318000, China

Abstract: TiAl alloy was mixed with BN nanoplates and then sintered at 1300 °C through spark plasma sintering technique, and the hybrid TiB₂-Ti₂AlN/TiAl composites were in-situ prepared. The microstructural evolution and mechanical properties at room temperature of TiAl composites were investigated. Results show that a fully lamellar microstructure can be achieved in the TiAl composites with BN nanoplates of lower content, whereas a transformation to the nearly lamellar microstructure can be observed under higher BN nanoplate content conditions. The microstructure of TiAl composites is significantly refined due to the even distribution of in-situ prepared TiB₂-Ti₂AlN particles at the lamellar colony boundaries. Notably, a continuous core-shell structure of TiB₂-Ti₂AlN particles is formed at the lamellar grain boundary after adding 0.5wt% BN nanoplates. The results of compression and friction wear at room temperature show that the hardness and compressive strength of TiAl composites are greatly improved with the increase in BN nanoplate content from 0wt% to 1wt%. Meanwhile, the average coefficient of friction decreases from 0.59 to 0.47, and the wear rate decreases by 29.9%. These remarkable mechanical properties are mainly attributed to the strengthening effects of the in-situ formation of TiB₂-Ti₂AlN particles, refined microstructure, and core-shell structure.

Key words: TiAl composite; TiB₂-Ti₂AlN particle; SPS; mechanical properties

TiAl alloys attract much attention due to their exceptional properties, including lightweight construction and excellent creep/corrosion resistance^[1-3], presenting great potential for applications in lightweight structures, aerospace, and automobile industries^[4]. However, their widespread application is often restricted by inferior mechanical properties, particularly the strength and ductility. Recently, the methods for enhancement in mechanical properties of TiAl alloys have been researched. Various techniques, such as heat treatment^[5-6], thermal-mechanical processing^[7], alloying^[8-9], and composite techniques^[10-17], have been employed to improve the mechanical properties of TiAl alloys.

Introducing various ceramic particles (TiB₂^[10], Ti₅Si₃^[11], SiC^[12], WC^[13], TiC^[14], Ti₂AlC^[15-16], and Ti₂AlN^[17]) can reinforce TiAl alloys owing to the excellent synergy effect between the matrix and reinforcement. Notably, the mechanical properties of these composites are significantly affected by the characteristic of reinforcement (variety, morphology,

dispersion, and size). For example, the addition of TiB₂ particles can effectively enhance the strength of TiAl alloys but seriously reduce the ductility^[10]. It is reported that the strength of Ti₂AlN/TiAl composites is higher than that of TiAl alloys, but their ductility is similar. This strength improvement is primarily attributed to the unique layer structure of MAX phases ($M_{n+1}AlX_n$ with $n=1, 2, 3$, such as Ti₂AlC and Ti₂AlN), which possess combination properties of metal and ceramic^[17]. Therefore, it can be seen that the strength-ductility synergy of TiAl composites is inadequate with a single reinforcement phase. Dual-phase reinforcement with novel structure is expected to enhance the mechanical properties of TiAl alloys, simultaneously improving the strength and ductility.

In addition, the inferior tribological performance and fretting wear damage severely restrict the development of TiAl alloys^[18]. The insufficient tribological performance has adverse impacts on the surface morphology and service life, which leads to crack initiation and early failure under complex

Received date: January 01, 2024

Foundation item: National Natural Science Foundation of China (52171120, 52271106, 52071188); Zhejiang Province Natural Science Foundation (LZY22E010001)
Corresponding author: Ma Tengfei, Ph. D., Key Laboratory of Air-Driven Equipment Technology of Zhejiang Province, Quzhou University, Quzhou 324000, P. R. China, Tel: 0086-571-8026716, E-mail: 36105@qzc.edu.cn

Copyright © 2024, Northwest Institute for Nonferrous Metal Research. Published by Science Press. All rights reserved.

operating conditions^[19]. Therefore, enhancement in tribological properties of TiAl alloys is also important. Some researches suggested that the wear resistance of TiAl alloys could be enhanced through strengthening effects, because the tribological properties are interconnected with mechanical properties. Hence, the better the strength, the better the wear resistance^[20].

In this research, TiAl composites reinforced by dual-phase $\text{TiB}_2\text{-Ti}_2\text{AlN}$ particles were prepared by spark plasma sintering (SPS) technique. BN nanoplates were used as the source of B and N elements for the precipitation of $\text{TiB}_2\text{-Ti}_2\text{AlN}$ particles by an in-situ reaction with TiAl alloys during SPS process. The superior mechanical properties and good wear resistance of TiAl composites were obtained by in-situ hybrid $\text{TiB}_2\text{-Ti}_2\text{AlN}$ particles. This research investigated the impact of BN nanoplate content on the microstructure evolution and mechanical properties of TiAl composites, and the corresponding strengthening and wear mechanisms were also discussed.

1 Experiment

The raw materials consisted of pre-alloyed TiAl (Ti-48Al-2Nb-2Cr, at%) powder with diameter of 53–150 μm , which was provided by Xi'an Sailong AM Technologies Co., Ltd. BN nanoplates with sizes of 0.1–0.4 μm were purchased from XFNANO Co., Ltd. TiAl composites were prepared with 0.1wt%, 0.3wt%, 0.5wt%, and 1.0wt% BN nanoplates. Firstly, the TiAl pre-alloyed powders with different BN nanoplate contents were treated by ball milling at 300 r/min for 6 h and then by SPS process at 1300 °C and 45 MPa for 5 min. The sintered samples containing 0wt%, 0.1wt%, 0.3wt%, 0.5wt%, and 1.0wt% BN nanoplates were denoted as TiAl-0BN, TiAl-0.1BN, TiAl-0.3BN, TiAl-0.5BN, and TiAl-1.0BN, respectively.

The samples for compression tests were cut from the sintered ones with diameter of 4 mm and height of 6 mm. The

compression tests were conducted at room temperature and strain rate of 0.001 s^{-1} by MTS-370.10 testing machine. Before compression tests, the surfaces of each sample were polished by 2000# sandpaper and ultrasonically cleaned for 10 min. Three samples were tested under the same condition to ensure reliability of experiment results. Hardness of the TiAl composites was characterized by Vickers hardness tester (MVS-1000IMT2) with applied normal force of 5 N and holding time of 10 s. To obtain the average results, more than 10 points were selected and measured of each sample. Tribological behavior of TiAl composites was investigated by ball-on-plate tribometer (HT-1000) at room temperature and rotation speed of 600 r/min in air with sliding against Si_3N_4 balls of 6 mm in diameter. The experiments were conducted for 30 min with the wear radius of 5 mm and applied load of 5 N.

The initial sintered microstructure, fracture morphologies, and worn surfaces of the TiAl composites were observed by scanning electron microscope (SEM, HITACHI SU8010) equipped with energy-dispersive spectrometer (EDS). In addition, Keyence surface profilometer (VHX-2000) was used to characterize the profiles of worn surfaces. Besides, the microstructure analysis was further conducted by transmission electron microscope (TEM, Tecnai G2 F30, FEI, USA), and TEM sample was prepared by wire cutting and then ion milling.

2 Results and Discussion

2.1 Microstructure of sintered TiAl composites

Fig.1 displays SEM images of the sintered TiAl composites with different BN nanoplate contents. Fig.2 shows lamellar colony sizes and hardness results of sintered TiAl composites with different BN nanoplate contents. No discernible pores can be detected. This suggests that the TiAl composites possess a relatively high density through SPS process. The microstructures of the TiAl composites significantly change

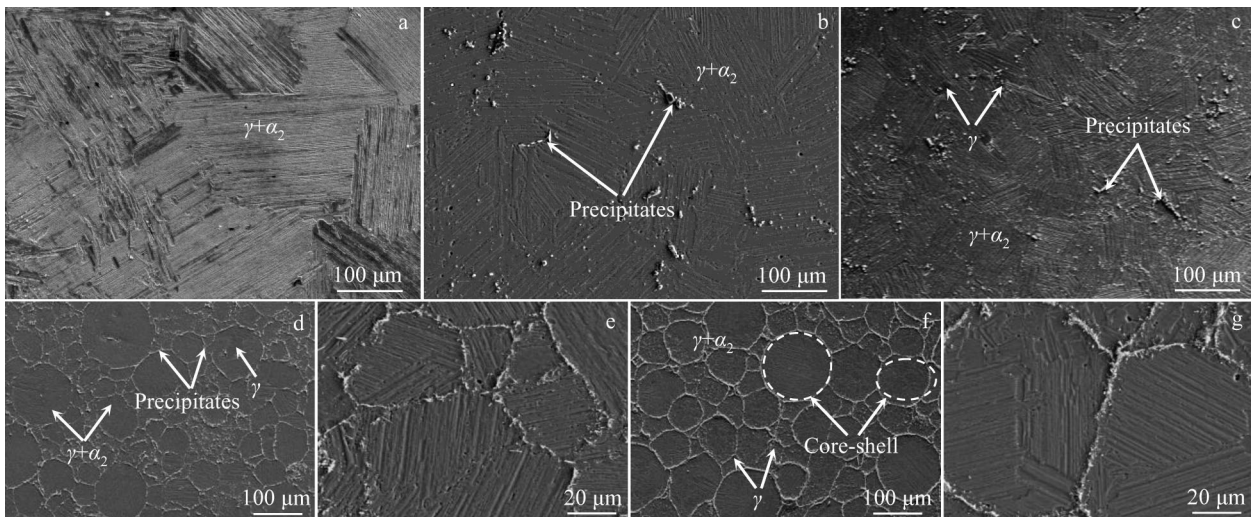


Fig.1 SEM images of TiAl composites with different BN nanoplate contents after SPS at 1300 °C: (a) TiAl-0BN, (b) TiAl-0.1BN, (c) TiAl-0.3BN, (d) TiAl-0.5BN, and (f) TiAl-1.0BN samples; enlarged images of Fig.1d (e) and Fig.1f (g)

after the addition of BN nanoplates, as shown in Fig. 1a–1e. In this research, the sintering temperature (1300 °C) is related to the single α phase region in phase diagram, where a fully lamellar microstructure can be obtained through the transformation of $\alpha \rightarrow \gamma + \alpha \rightarrow$ lamellar ($\gamma + \alpha_2$) phase after sintering^[4]. Obviously, the TiAl alloy without BN exhibits a fully lamellar microstructure composed of $\alpha_2 + \gamma$ lamellae with an average lamellar colony size of about 241.6 μm , as shown in Fig. 1a and Fig. 2. However, the TiAl-0.1BN and TiAl-0.3BN alloys show a fully lamellar microstructure with refined lamellar colonies, and some white precipitates can be observed at the lamellar colony boundaries, as shown in Fig. 1b–1c. With the increase in BN nanoplate content to 0.5wt%, it can be found that a large number of precipitates are aggregated at the lamellar colony boundaries, forming a continuous core-shell structure, as shown in Fig. 1d. Wang^[21] and Tan^[22] et al reported that the novel core-shell structures have a significant effect on the mechanical properties of metal matrix composites, which can improve both the strength and plasticity. Besides, it is clear that the TiAl-0.5BN and TiAl-1.0BN alloys have a nearly lamellar microstructure consisting of lamellar colonies and equiaxed γ grains, as shown in Fig. 1e and 1g, respectively. This phenomenon is mainly attributed to the increase in phase transformation temperature T_a ($\gamma \rightarrow \alpha$) of TiAl alloys, which is induced by BN nanoplates of high content, leading to an incomplete transformation ($\gamma \rightarrow \alpha$) at the same sintering temperature. During SPS, the BN nanoplates of high content distributed on the TiAl powder surfaces can hinder the heat transfer and mass transfer between different powders. Moreover, the in-situ synthesized ceramic particles inhibit the $\gamma \rightarrow \alpha$ transformation through pinning effect on the grain boundaries. Besides, the interstitial alloying elements, such as C, B, and N, can increase T_a of TiAl alloys, resulting in incomplete $\gamma \rightarrow \alpha$ transformation^[23–24].

According to the lamellar colony sizes and hardness results in Fig. 2, it can be seen that the lamellar colony size is decreased and hardness is increased with the increase in BN nanoplate content. This is mainly attributed to the effective pinning of grain boundaries by precipitates, which hinders the grain boundary migration, ultimately suppressing

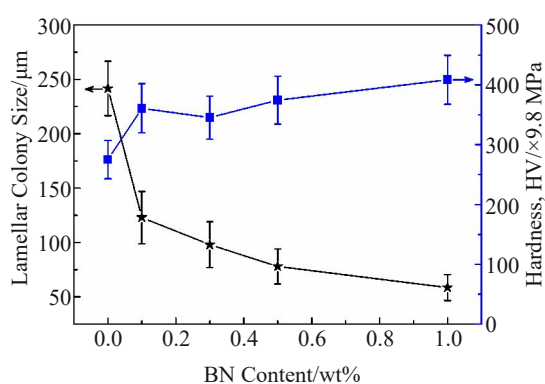


Fig.2 Lamellar colony sizes and hardness results of TiAl composites with different BN nanoplate contents after SPS at 1300 °C

the grain growth and resulting in a more refined and homogeneous microstructure^[23]. Notably, the lamellar colony size decreases from 241.6 μm to 58.6 μm when the BN nanoplate content increases from 0wt% to 1.0wt%. Furthermore, the TiAl-1.0BN alloy has the maximum hardness of about 3974.9 MPa, increasing by 39.1% compared with that of TiAl-0BN alloy.

TEM and high resolution TEM (HRTEM) were used to characterize the morphologies of TiAl-0.5BN alloy and to further determine the precipitates. The bright field-TEM (BF-TEM) image of TiAl-0.5BN alloy is shown in Fig. 3a, which reveals that the lamellar microstructure ($\gamma + \alpha_2$) and nanometer-sized precipitates are distributed in the lamellar colony boundaries. Notably, a large number of dislocations can be observed in the TiAl matrix. The high angle annular dark field-scanning transmission electron microscope (HAADF-STEM) image of TiAl-0.5BN alloy is displayed in Fig. 3b, and the corresponding EDS mapping analyses in Fig. 3c reveal that the precipitates are mainly composed of Ti, B, and N, indicating the in-situ synthesis of borides and nitrides during SPS process. Fig. 3d–3g show HRTEM images and corresponding fast Fourier transform (FFT) patterns. According to FFT results, it is evident that the borides and nitrides correspond to the TiB_2 and Ti_2AlN phases, respectively.

2.2 Mechanical properties

The compressive properties and tribological behavior of TiAl composites with different BN nanoplate contents were evaluated at room temperature to study the influence of BN nanoplate content on the mechanical properties. Fig. 4a displays the engineering stress-engineering strain curves, and the compressive strength and fracture strain of TiAl composites at room temperature are shown in Fig. 4b. Three stages can be recognized in the compressive deformation behavior: (1) the elastic deformation stage prior to yielding, where the engineering stress is rapidly increased with the increase in engineering strain; (2) the plastic deformation stage after yield, where the plastic deformation occurs and the engineering stress is increased slowly with the increase in strain; (3) the fracture stage at the end of deformation, where brittle fracture occurs. Obviously, the yield strength of TiAl composites is significantly higher than that of TiAl alloy without BN addition, indicating that the substantial enhancement in the elastic modulus of TiAl alloy results from the addition of reinforcement phases. The TiB_2 - Ti_2AlN particles in TiAl composites can bear the load, hinder the crack propagation, and simultaneously improve strength and plasticity. In addition, the microstructure of the TiAl composites is also refined after the addition of reinforcement phases, resulting in the refinement strengthening effect^[12,15].

Fig. 4b exhibits the corresponding mechanical properties of TiAl composites. The TiAl-1.0BN alloy exhibits the optimal performance: the maximum compressive strength of 2084.3 MPa and the relatively lower fracture strain of 29.1%. The maximum compressive strength of TiAl-1.0BN alloy improves by 16.5%, compared with that of TiAl-0BN alloy. Remarkably, the compressive strength of TiAl-1.0BN alloy is

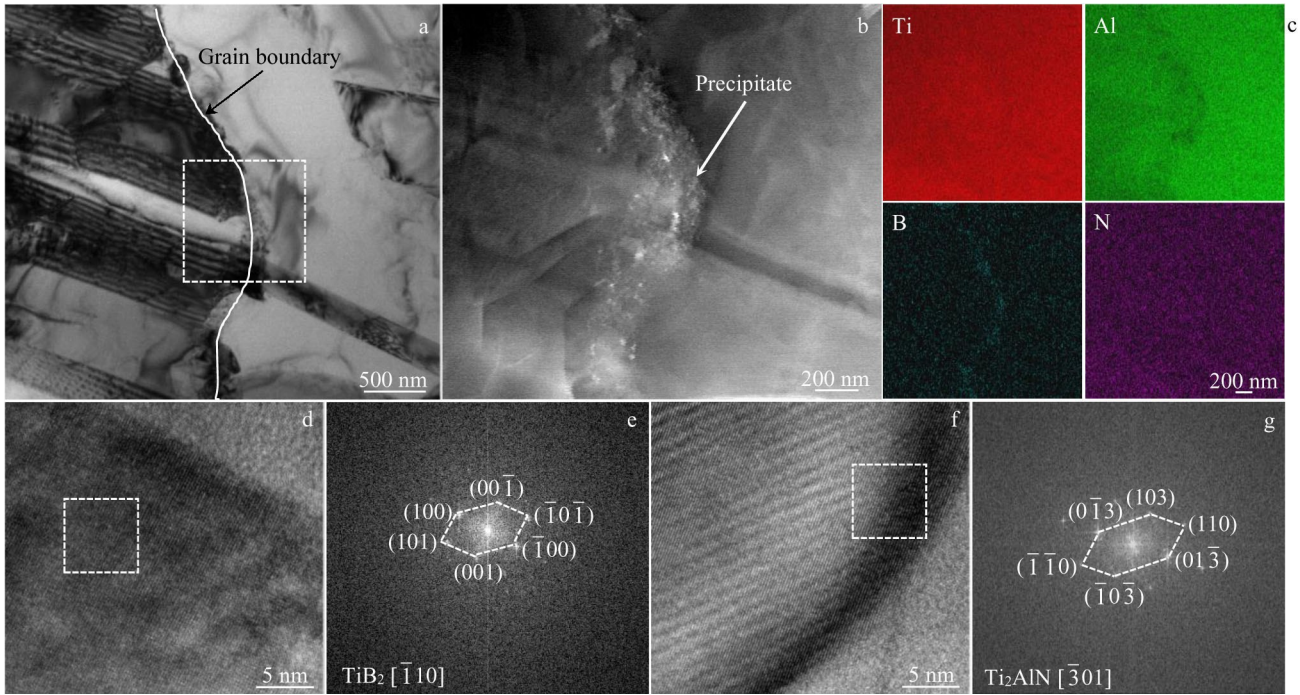


Fig.3 BF-TEM image (a), HAADF-STEM image (b), and corresponding EDS element mapping results (c) of TiAl-0.5BN alloy; HRTEM images of TiB_2 (d) and Ti_2AlN (f) phases; FFT patterns of square areas in Fig.3c (e) and Fig.3d (g)

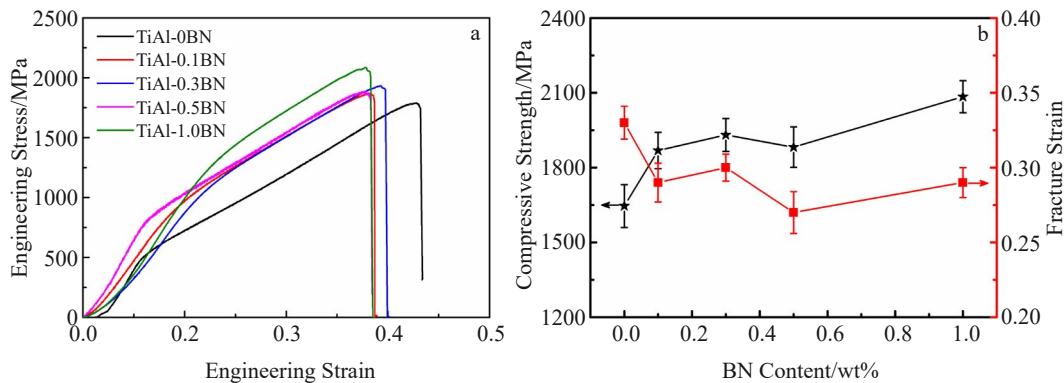


Fig.4 Compressive properties of TiAl composites: (a) engineering stress-engineering strain curves; (b) compressive strength and fracture strain

even higher than that of Ti-48Al-2Nb-2Cr alloy with fully lamellar structure (1510 MPa) prepared by hot isostatic pressing and heat treatment^[8]. This enhancement can be attributed to the refined lamellar colonies and the unique core-shell structure appearing in the alloy. In addition, it is noteworthy that the fracture strain of TiAl composites slightly decreases compared with that of TiAl alloy. This is because the hard-brittle phases appear at the lamellar colony boundaries in the composites, which are more likely to cause stress concentration and fracture^[15].

Fig.5 shows the coefficient of friction (COF) curves of TiAl composites at room temperature. The addition of BN nanoplates results in a significant decrease in COF, which is primarily attributed to the refined lamellar colonies and the core-shell structure. The average COF of TiAl-0BN, TiAl-0.1BN, TiAl-0.3BN, TiAl-0.5BN, and TiAl-1.0BN alloys is

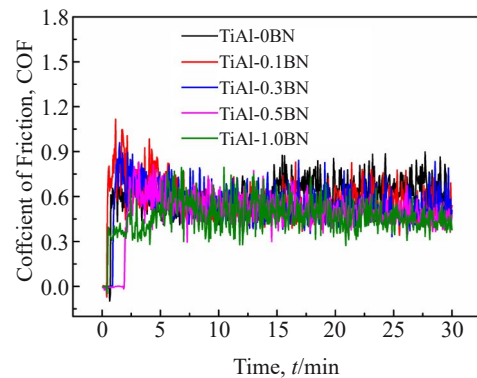


Fig.5 COF curves of TiAl composites

0.59, 0.56, 0.54, 0.49, and 0.47, respectively. Notably, the TiAl-1.0BN alloy possesses the minimum average COF as

0.47, and average COF of TiAl alloy at room temperature is 0.59. As reported in Ref. [18, 20], tribological properties are significantly influenced by the mechanical properties, including hardness, strength, and plasticity. Typically, the correlation between mechanical properties and tribological properties can be expressed by the equation $W=k(P/H)$, where W represents wear rate, H is hardness, P is applied load, and the constant k is related to plasticity^[20]. According to the results, the hardness and compressive strength are improved by the addition of BN without seriously sacrificing plasticity. Hence, TiAl composites containing BN nanoplates exhibit superior tribological properties, compared with TiAl alloy without BN addition.

2.3 Microstructure evolution and wear mechanism

Normally, cracks are preferentially initiated at the grain boundaries and interfaces of lamellae in TiAl alloy due to the stress concentration and insufficient bonding strength. Subsequently, the cracks are propagated along the grain boundaries and lamellae interfaces during the compression test. However, it is well known that hetero-structured materials are regarded as one of the most promising structural materials due to their extraordinary mechanical properties^[25-27], which provides a new strategy to break the strength-ductility balance of metal materials. In this research, the improvement in strength of TiAl composites can be attributed to the formation of high strengthening ceramic particles and core-shell structure deformation-induced strengthening, which result from the heterogeneous deformation between nanoparticles (shell) and TiAl alloy (core)^[27]. Furthermore, the nanoparticles (shell) distributed at the lamellar grain boundaries can inhibit the dislocation movement and crack propagation, enhancing the uniform deformability and strain hardening of TiAl composites.

The compressive fracture morphologies of TiAl composites show typical brittle fracture characteristics, as shown in Fig. 6. For TiAl alloy, typical grain boundary cracks can be observed, as shown in Fig. 6a. Interestingly, the TiAl composites show the cleavage fracture morphologies, including tongue pattern, river pattern, and tearing edge, as shown in Fig. 6b – 6e. Notably, the introduction of TiB₂-Ti₂AlN particles cannot only refine the microstructure but also hinder the crack propagation, causing the crack deflection during deformation and then resulting in the strengthening effect (Fig. 6d). Furthermore, with the formed core-shell structure and 0.5wt% BN nanoplates, the TiB₂-Ti₂AlN particles (shell) can bear more stress and coordinate more deformation, simultaneously strengthening and toughening the TiAl composites^[21]. In addition, the TiB₂-Ti₂AlN particles are easier to pull out under high stress conditions (Fig. 6e), which contributes to higher toughening effect through absorbing energy and delaying fracture. Therefore, the reduction in fracture strain of the TiAl composites is not obvious even after adding a large number of BN nanoplates.

In order to further determine the wear volume (V) and wear rate (W) of TiAl composites after wear tests, the worn surface profiles were characterized by Keyence surface profilometer (VHX-2000), and the results are shown in Fig. 7. The wear width and depth of the worn tracks can be directly measured, and the corresponding values of V and W are calculated through $V=AL$ and $W=V/SN$, where A represents the cross-sectional area, L donates the perimeter of worn track, S denotes the sliding distance, and N stands for the applied load^[15]. The wear properties (wear width, wear depth, V , and W) are calculated and listed in Table 1. It is obvious that both V and W are significantly decreased with the increase in BN nanoplate content. Moreover, the W value of TiAl-1.0BN alloy

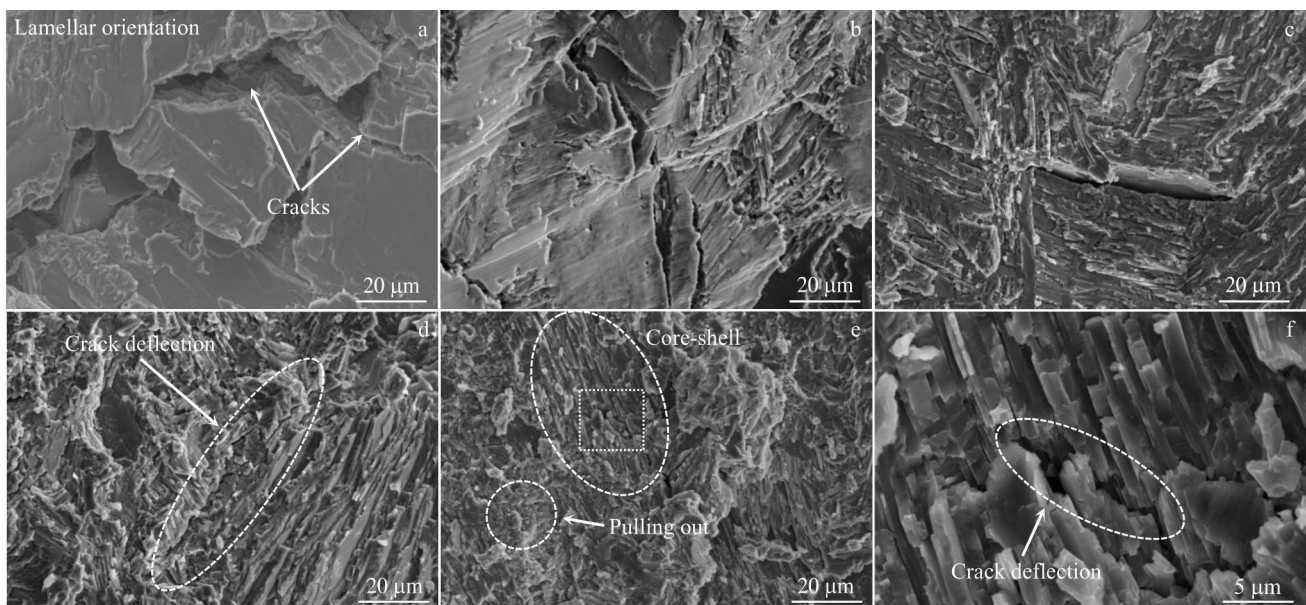


Fig.6 Fracture morphologies of TiAl composites with different BN nanoplate contents after SPS at 1300 °C: (a) TiAl-0BN, (b) TiAl-0.1BN, (c) TiAl-0.3BN, (d) TiAl-0.5BN, and (e) TiAl-1.0BN samples; magnified image of marked rectangular area in Fig.6e (f)

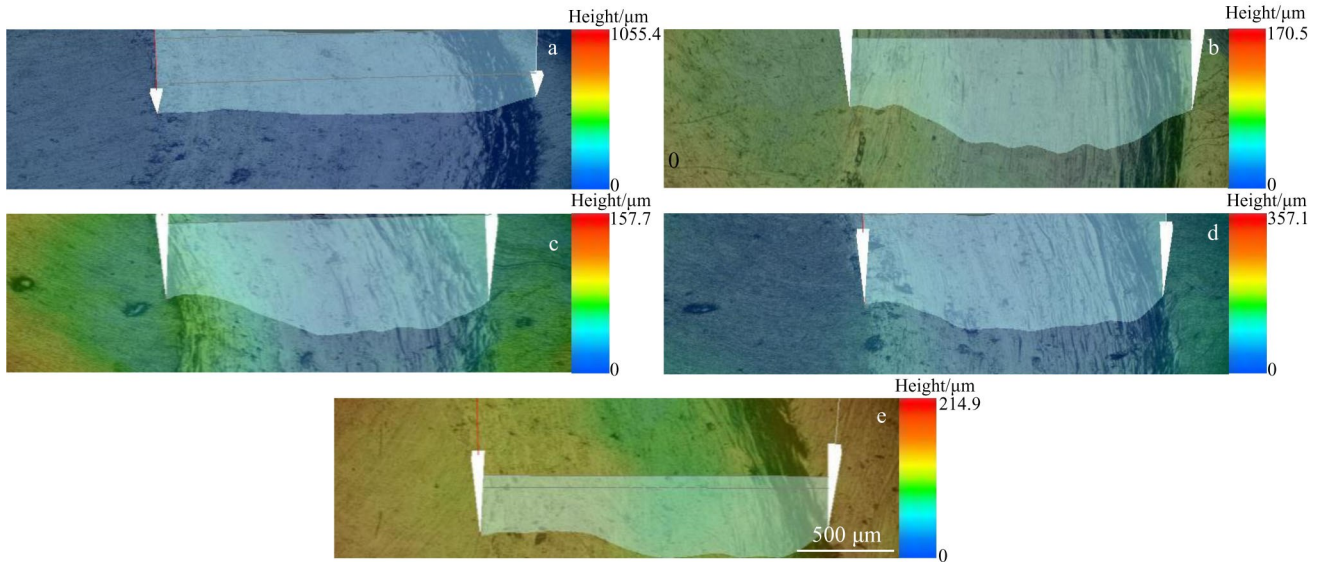


Fig.7 Worn surfaces of TiAl composites with different BN nanoplate contents after SPS at 1300 °C and corresponding 2D cross-section profiles of wear tracks: (a) TiAl-0BN, (b) TiAl-0.1BN, (c) TiAl-0.3BN, (d) TiAl-0.5BN, and (e) TiAl-1.0BN

Table 1 Room-temperature wear properties of TiAl composites with different BN nanoplate contents after SPS at 1300 °C

Wear property	TiAl-0BN	TiAl-0.1BN	TiAl-0.3BN	TiAl-0.5BN	TiAl-1.0BN
Average COF	0.59	0.56	0.54	0.49	0.47
Wear width/ μm	2084.6	1822.6	1817.2	1660.3	1902.6
Wear depth/ μm	64.54	66.23	58.70	54.75	48.65
Wear volume, V/mm^3	2.453	2.103	1.989	1.887	1.713
Wear rate, $W/\times 10^{-4} \text{mm}^3 \cdot \text{N}^{-1} \cdot \text{m}^{-1}$	2.17	1.86	1.76	1.67	1.52

is about 70.04% of that of TiAl-0BN alloy at room temperature. Comprehensively, the TiAl-1.0BN alloy shows the lowest COF (0.47), the smallest wear volume (1.713mm^3), and the slowest wear rate ($1.52 \times 10^{-4} \text{mm}^3 \cdot \text{N}^{-1} \cdot \text{m}^{-1}$). The wear rate of TiAl-1.0BN alloy decreases by 29.9%, compared with that of TiAl-0BN alloy. The results reveal a remarkable enhancement in the wear resistance of TiAl alloy, which is attributable to the in-situ synthesized TiB_2 - Ti_2AlN particles, the refined lamellar colonies, and the formed novel core-shell structure.

SEM characterizations and corresponding EDS analysis of the worn surfaces after wear test were conducted to explore the wear mechanism of TiAl composites. According to Fig. 8, it can be found that all TiAl composites display the typical furrow patterns on the worn surfaces. These furrows, caused by the micro-cutting and furrowing actions of the harder asperities on the Si_3N_4 ball during sliding, consist of grooves and wear debris parallel to the sliding direction. This phenomenon suggests that ploughing wear is the primary wear mechanism in this case^[18-19]. Furthermore, the worn surfaces of TiAl composites with BN addition exhibit smoother textures with reduced debris and smaller grooves, than that of the TiAl alloy without BN nanoplates, as shown in Fig. 8a–8e. This improvement can be attributed to the enhanced strength of TiAl composites, which results from their refined lamellar

colonies and novel core-shell structure. Typically, the refined lamellar colonies and core-shell structure can effectively hinder the movement of dislocations, leading to higher dislocation density and larger strain hardening, which further improves the wear resistance of TiAl composites^[28]. Fig. 8f–8i show SEM morphology and corresponding EDS mapping results of the worn surface of TiAl-0.5BN sample. The uniform distribution of B, N, and Si atoms on the surface indicates that during the wear test process, the harder asperities of the Si_3N_4 ball penetrate the softer surface of the TiAl composites, resulting in the formation of grooves and wear debris^[18].

The wear debris on the worn surfaces of TiAl-0BN and TiAl-1.0BN samples was collected after wear test and then examined by SEM and EDS, and the results are shown in Fig. 9 and listed in Table 2, respectively. It can be found that the characteristic of wear debris barely changes after the addition of BN nanoplates, which consists of a large amount of debris (approximately $10 \mu\text{m}$) with fragments of fine particles (approximately $1 \mu\text{m}$). The formation of wear debris indicates that severe wear deformation occurs at the surfaces of TiAl-0BN and TiAl-1.0BN samples during sliding wear. In addition, it is also worth noting that the O and Si element contents are relatively large in the wear debris, as shown in Table 2, suggesting that the wear debris contains TiAl matrix,

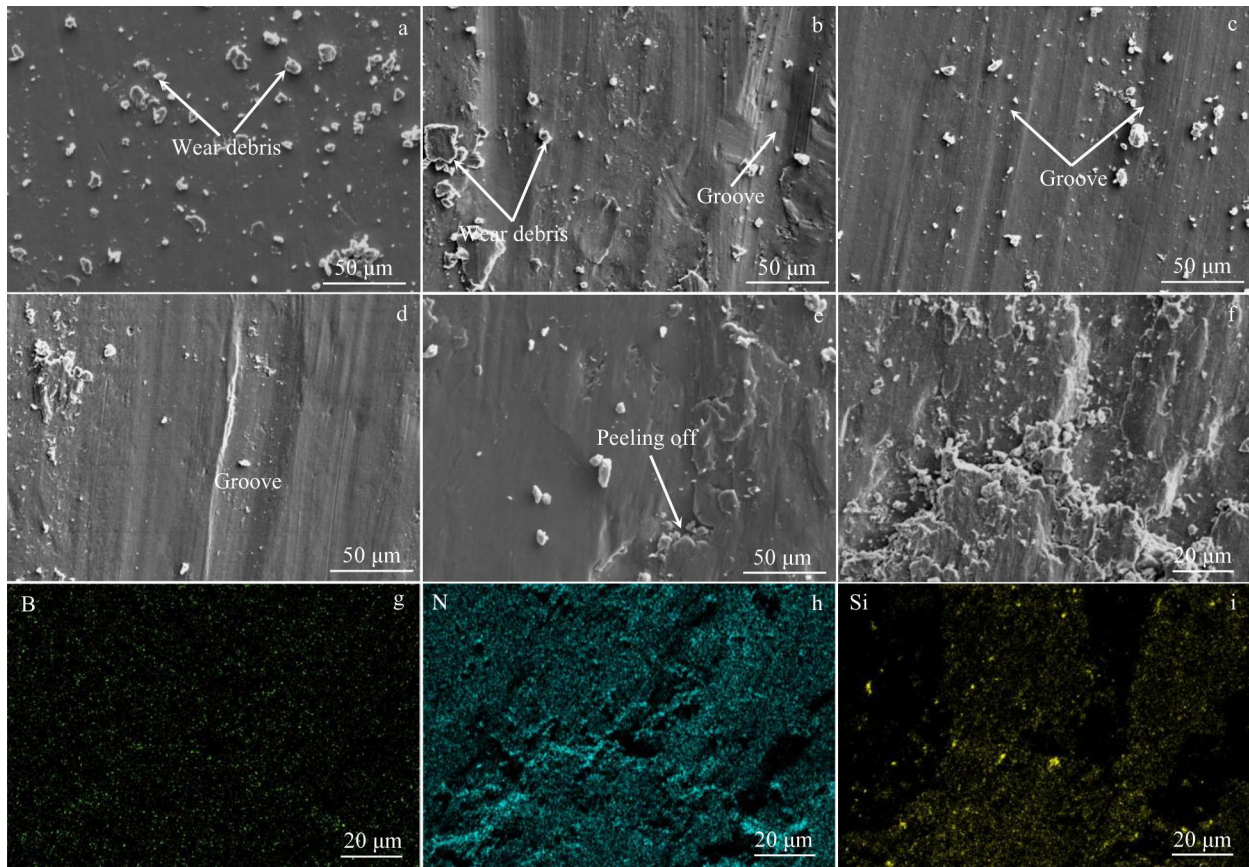


Fig.8 SEM images of worn surfaces of TiAl composites with different BN nanoplate contents after SPS at 1300 °C: (a) TiAl-0BN, (b) TiAl-0.1BN, (c) TiAl-0.3BN, (d,f) TiAl-0.5BN, and (e) TiAl-1.0BN samples; EDS mapping results of Fig.8f: (g) B element, (h) N element, and (i) Si element

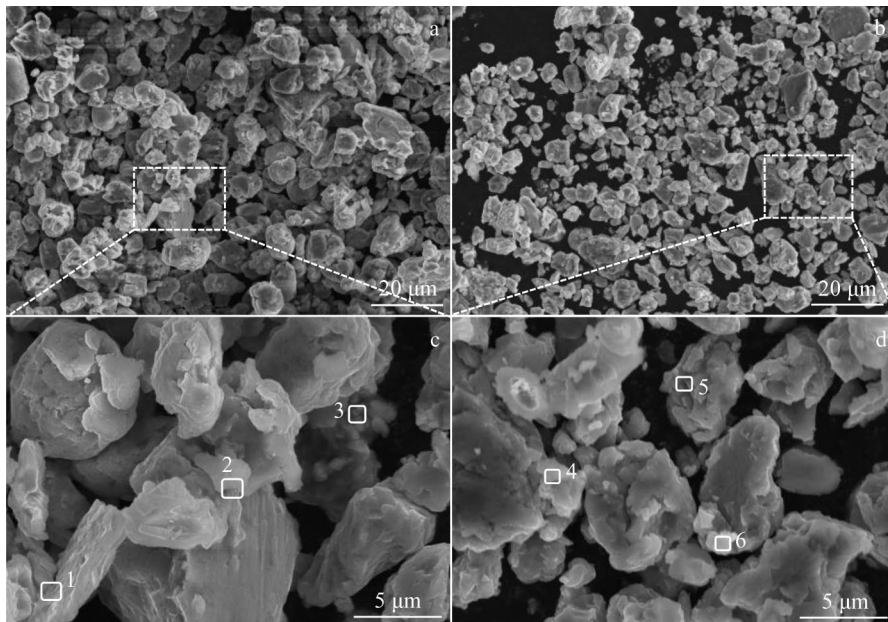


Fig.9 SEM images of wear debris of TiAl-0BN (a, c) and TiAl-1.0BN (b, d) samples after friction

Si₃N₄, and oxidized products.

Fig.10 illustrates the synthesis and wear mechanism of the TiAl composites with different BN nanoplate contents. After

mixing by mechanical ball milling, the BN nanoplates are uniformly distributed on the surface of spherical TiAl powder. A fully lamellar microstructure can be observed in both the

Table 2 EDS results of different points on wear debris in Fig. 9 (at%)

Position	Ti	Al	Nb	Cr	O	Si
Point 1	26.73	28.00	0.73	1.21	42.31	1.03
Point 2	32.26	29.07	0.71	1.41	36.03	0.52
Point 3	50.89	16.48	0.03	3.54	28.79	0.27
Point 4	20.74	22.63	2.15	0.47	39.40	0.96
Point 5	26.54	26.62	0.68	1.37	40.82	0.39
Point 6	27.02	28.67	0.71	1.43	38.93	0.41

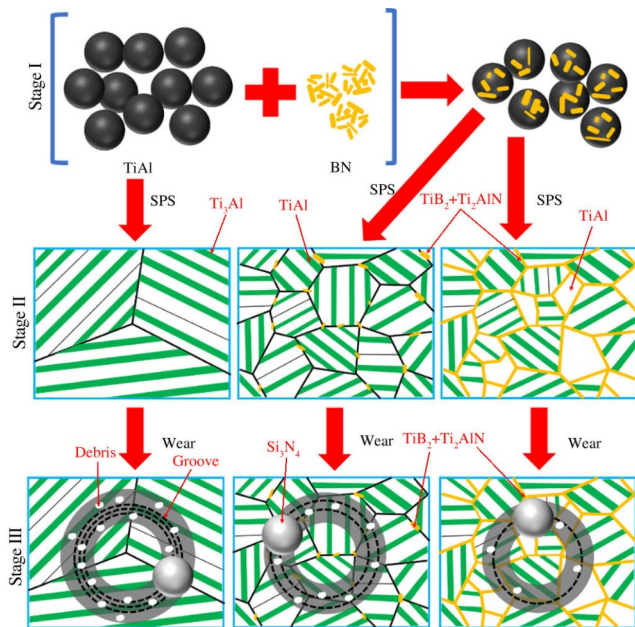


Fig.10 Schematic diagrams and mechanism of tribological behavior of TiAl composites with BN nanoplates

pure TiAl alloy and the TiAl composite containing a small number of BN nanoplates. In the meantime, the nearly lamellar microstructure with the novel continuous core-shell structure is formed with the increase in BN nanoplate content from 0wt% to 0.5wt%, as shown in Fig.1 and the stage II in Fig.10. Besides, the $\text{TiB}_2\text{-Ti}_2\text{AlN}$ particles are in-situ formed and distributed at the lamellar colony boundaries with the addition of BN nanoplates. During SPS, primary ceramic particles (nitride, boride) are initially precipitated at the boundaries of TiAl powder by in-situ reactions between the BN nanoplates and TiAl matrix with the increase in temperature. The precipitation of nitride and boride particles is mainly attributed to the low solid solubility of interstitial atoms in the $\gamma\text{-TiAl}$ phase and $\alpha_2\text{-Ti}_3\text{Al}$ phase. After SPS process, the phase transformation of $\alpha \rightarrow \alpha + \gamma \rightarrow \text{lamellar } (\alpha_2 + \gamma)$ phase occurs, and the primary boride (TiB_2) and nitride (Ti_2AlN) are still distributed at the lamellar colony boundaries, forming a continuous core-shell structure. Particularly, the core-shell structure of TiAl alloy prepared by rapid-heating SPS may change during long-term high temperature service. Firstly, the TiAl alloy suffers the lamellar decomposition, phase transformation, and grain coarsening during long-term

high temperature service. Secondly, the bonding strength of ceramic particles and matrix is decreased and the plastic deformation is obvious at high temperatures, which results in the partial peeling of the ceramic particles from the matrix. Therefore, it is possible that the core-shell structure of TiAl alloy changes at high temperature. For TiAl alloy, the softer matrix is severely penetrated by the harder Si_3N_4 ball during sliding, resulting in significant furrows on the alloy surface and leading to peeling off phenomenon in the grooves (stage III in Fig.10). These factors contribute to the decrease in wear resistance and the increase in wear volume.

However, the introduction of BN nanoplates to the TiAl alloy causes the formation of in-situ $\text{TiB}_2\text{-Ti}_2\text{AlN}$ particles during sintering. The presence of fine and stable $\text{TiB}_2\text{-Ti}_2\text{AlN}$ precipitates substantially enhances the strength and wear resistance of the TiAl composites. Furthermore, the mechanical properties of the TiAl composites can also be improved by the novel core-shell structure^[21-22]. These enhancements lead to the reduction in both depth and width of the wear tracks, as well as the roughness of wear surfaces. Hence, the enhanced mechanical properties and wear resistance of $\text{TiB}_2\text{-Ti}_2\text{AlN/TiAl}$ composites can be primarily attributed to the in-situ $\text{TiB}_2\text{-Ti}_2\text{AlN}$ particles, refined lamellar colonies, and novel core-shell structure.

3 Conclusions

1) $\text{TiB}_2\text{-Ti}_2\text{AlN}$ particles reinforced TiAl composites with a fully lamellar refined microstructure can be achieved at low BN nanoplate content, whereas the nearly lamellar microstructure and the novel continuous core-shell structure are formed when the BN nanoplate content reaches 0.5wt%.

2) The mechanical properties of the Ti-48Al-2Cr-2Nb alloy are improved by the in-situ $\text{TiB}_2\text{-Ti}_2\text{AlN}$ particles and novel core-shell structure. The TiAl-1.0BN sample shows a significant improvement in both hardness (3974.9 MPa) and maximum compressive strength (2084.3 MPa), which improve by 39.1% and 16.5%, respectively, compared with those of TiAl alloy without BN addition.

3) The COF value, wear volume, and wear rate of the TiAl composites are decreased with the increase in BN nanoplate content. The TiAl-1.0BN alloy shows the lowest COF (0.47), the smallest wear volume (1.713 mm^3), and the slowest wear rate ($1.52 \times 10^{-4} \text{ mm}^3 \cdot \text{N}^{-1} \cdot \text{m}^{-1}$). The improvement in mechanical performances and wear resistance are mainly attributed to the strengthening effects induced by the $\text{TiB}_2\text{-Ti}_2\text{AlN}$ particles, refined lamellar colonies, and novel core-shell structure.

References

- 1 Ding Jie, Zhang Minghe, Liang Yongfeng et al. *Acta Materialia*[J], 2018, 161: 1
- 2 Liu Chengze, Wang Yupeng, Han Weizhong et al. *ACS Applied Materials & Interfaces*[J], 2022, 14: 8394
- 3 Yang Jieren, Gao Zitong, Zhang Xiaogan et al. *Metallurgical and Materials Transactions A*[J], 2020, 51A: 5295

- 4 You Ruyue, Wang Qiang, Zhao Chunling. *Materials China*[J], 2023, 42(8): 669 (in Chinese)
- 5 Guo Yingchao, Liang Yongfeng, Lin Junpin. *Intermetallics*[J], 2023, 159: 107937
- 6 Liu Pei, Hou Bo, Wang Anqi et al. *Journal of Materials Science & Technology*[J], 2023, 159: 21
- 7 Tang Bin, Cheng Liang, Kou Hongchao et al. *Intermetallics*[J], 2015, 58: 7
- 8 Youn S J, Kim Y K, Kim H S et al. *Intermetallics*[J], 2023, 153: 107784
- 9 Wang Yupeng, Rong Guangfei, Ma Tengfei et al. *Journal of Materials Research and Technology*[J], 2024, 28: 1667
- 10 Wei Yuanzheng, Qiu Feng, Shu Shili et al. *Materials Science and Engineering A*[J], 2022, 845: 143214
- 11 Chen Ruirun, Ma Tengfei, Guo Jingjie et al. *Rare Metal Materials and Engineering*[J], 2017, 46(S1): 20 (in Chinese)
- 12 Tan Yingmei, Chen Ruirun, Fang Hongze et al. *Intermetallics*[J], 2018, 98: 69
- 13 Li Wei, Li Ming, Liu Jie et al. *Journal of Alloys and Compounds*[J], 2019, 770: 640
- 14 Wu Zeen, Hu Rui, Zhang Tiebang et al. *Materials Characterization*[J], 2017, 124: 1
- 15 Ma Tengfei, Li Qiaoyu, Wang Yupeng et al. *Intermetallics*[J], 2022, 146: 107563
- 16 Hou Bo, Liu Pei, Wang Anqi et al. *Vacuum*[J], 2022, 201: 111124
- 17 Liu Pei, Sun Dongli, Han Xiuli et al. *Materials & Design*[J], 2017, 130: 239
- 18 García-Martínez E, Miguel V, Martínez A et al. *Wear*[J], 2021, 484–485: 203992
- 19 Mengis L, Grimme C, Galetz M C. *Wear*[J], 2019, 426–427: 341
- 20 Cheng Jun, Yang Jun, Zhang Xinghua et al. *Intermetallics*[J], 2012, 31: 120
- 21 Wang Yupeng, Ma Tengfei, Chen Zhanxing et al. *Materials Science and Engineering A*[J], 2024, 889: 145873
- 22 Tan Chaolin, Zou Ji, Wang Di et al. *Composites Part B: Engineering*[J], 2022, 236: 109820
- 23 Lapin J, Kamyshnykova K, Pelachová T et al. *Intermetallics*[J], 2021, 128: 107007
- 24 Ghorbani H R, Kermanpur A, Rezaeian A et al. *Materials Today Communications*[J], 2020, 25: 101494
- 25 Ding Hao, Cui Xiping, Zhang Yuanyuan et al. *International Journal of Plasticity*[J], 2023, 171: 103805
- 26 Ding Hao, Cui Xiping, Wang Zhiqi et al. *Journal of Materials Science & Technology*[J], 2022, 107: 70
- 27 Yu Yonghao, Kou Hongchao, Wang Yichao et al. *Acta Materialia*[J], 2023, 255: 119036
- 28 Shi Yeqi, Szlufarska I. *Acta Materialia*[J], 2020, 200: 432

原位析出 TiB₂-Ti₂AlN 增强 TiAl 合金力学性能

王玉鹏¹, 李思颖¹, 马腾飞¹, 王晓红¹, 董多^{1,2}, 朱冬冬^{1,2}

(1. 衢州学院 浙江省空气动力装备技术重点实验室, 浙江 衢州 324000)

(2. 台州学院 材料科学与工程学院, 浙江 台州 318000)

摘要: 采用放电等离子烧结技术对 TiAl 合金和 BN 纳米片混合粉末在 1300 °C 下进行烧结, 原位合成了 TiB₂-Ti₂AlN/TiAl 复合材料, 并对 TiAl 复合材料的显微组织演变和室温力学性能进行了研究。结果表明, 添加低含量 BN 纳米片的 TiAl 复合材料为全片层组织, 而添加高含量 BN 纳米片的 TiAl 复合材料向近片层组织转变。此外, 原位合成的 TiB₂-Ti₂AlN 颗粒均匀分布在片层团晶界处, 显著细化了复合材料组织。当添加质量分数为 0.5% 的 BN 纳米片时, TiB₂-Ti₂AlN 颗粒在片层团晶界处形成连续核壳结构。室温压缩和摩擦磨损结果表明, 随着 BN 纳米片质量分数从 0% 增加到 1%, TiAl 复合材料的显微硬度和抗压缩强度显著提高, 摩擦磨损系数从 0.59 降低到 0.47, 磨损率降低了 29.9%。TiAl 复合材料优异的力学性能主要归因于原位析出的 TiB₂-Ti₂AlN 颗粒、细化的显微组织和核壳结构所产生的强化效应。

关键词: TiAl 复合材料; TiB₂-Ti₂AlN 颗粒; 放电等离子烧结; 力学性能

作者简介: 王玉鹏, 男, 1994 年生, 博士生, 衢州学院浙江省空气动力装备技术重点实验室, 浙江 衢州 324000, 电话: 0571-8026716, E-mail: wyp10279035@163.com